Pozzolanic Reactivity and Hydration Products of Cementitious Material Prepared Using Molybdenum Tailings

Biyao Geng [1], Zongwen Wang [2], Shihu Shi [1,*], Kun Wang [3], Jianxun Fu [1], Zhenjiang Wen [1] and Xiaogang Guo [1]

1   China ENFI Engineering Co., Ltd., Beijing 100038, China
2   Zhaojin Mining Industry Co., Ltd., Zhaoyuan 265400, China
3   Institute of Technical Information for Building Materials Industry, Beijing 100024, China
*   Correspondence: shish@enfi.com.cn; Tel.: +86-010-6393-6326

Abstract: This study aimed to examine the pozzolanic reactivity and hydration products of cementitious materials prepared using molybdenum tailings. During the grinding process, the particle size of molybdenum tailings decreases continuously between 15 and 60 min, and the specific surface area increases from 367 to 932.4 m^2/kg. For this, samples were prepared using 91 wt% milled molybdenum tailings, 3 wt% natural gypsum, 6 wt% calcium hydroxide, and a mixture of 0.3 wt% water reducer and water:binder at a ratio of 0.2. The phase transformation and hydration products of molybdenum tailings were analyzed using a compressive strength tester, X-ray diffraction, scanning electron microscopy, and infrared radiation. The 3-, 7-, and 28-day compressive strengths of the samples were found to be 1.67, 3.17, and 3.83 MPa, respectively, which shows that the molybdenum tailings have pozzolanic reactivity. Other testing means showed that the molybdenum tailings are mainly composed of ettringite and C-S-H gel under standard curing conditions, and the collaborative generation process of ettringite and C-S-H gel may exist in this system.

Keywords: molybdenum tailings; pozzolanic reaction; hydration; ettringite; C-S-H gel

1. Introduction

China has the largest molybdenum reserve in the world, which accounts for 8.4 million tons of the global molybdenum reserve [1]. With the rapid development of the national economy, the demand for molybdenum metal has gradually increased. Accordingly, the country's mining and processing capacity of molybdenum ore have also increased rapidly.

Molybdenum reserves in China are characterized by large proved reserves and low grade. At present, 65% of the total molybdenum deposits in the country are low-grade deposits that have an average grade of less than 0.1% [1]. Rich ore reserves with grades of more than 0.3% account for only 1% of the total reserves in the country. Molybdenum ore has a generally low raw ore grade. Therefore, the tailings ratio is high in the beneficiation process, indicating that more than 95% of the ore mining volume is discharged with tailings. These molybdenum tailings occupy a large number of land resources and increase the construction and maintenance funds of tailing ponds. Nevertheless, these tailings also pollute the surrounding water and soil, causing great safety hazards to the surrounding residential environment. The implementation of the government's "double carbon" policy and the continuous strengthening of environmental protection policies have restricted the construction of new tailing ponds in most regions of the country. Therefore, mining enterprises face the problem of insufficient tailing absorption capacity, which seriously restricts the sustainable development of enterprises and the regional economy.

Di Yanqing et al. [1–3] prepared lightweight, exterior-wall, thermal insulation materials with a fireproof performance up to the A1 level using ground molybdenum tailings powder, supplemented by other solid waste materials. Guo Xianjun et al. [4] produced high-quality cement clinker using molybdenum tailings as cement raw materials. Cui

Xiaowei et al. [5,6] studied the technology of concrete mixed with molybdenum tailings, and the compressive strength of the concrete mixed with a high-efficiency water reducing agent can reach 45.5 MPa at the age of 28 days. The incorporation of high-efficiency water reducing agents helps to improve the mechanical properties of concrete [7]. Research on pozzolanic activity and hydration products of a single component of molybdenum tailings has not been reported.

In this regard, utilizing molybdenum tailings to prepare tailing cementitious materials can conserve the amount of cement used in concrete, reduce the impact of the cement industry on the environment, and reduce production costs. Such an approach can also solve a series of problems caused by tailing stockpiling and improve the product-added value of tailings. Therefore, in this study, a purified slurry test block was made using ground molybdenum tailings, gypsum, and calcium hydroxide, and its pozzolanic reactivity was investigated. Its phase change was analyzed through X-ray diffraction (XRD), scanning electron microscopy (SEM), and infrared radiation (IR), and the hydration products of molybdenum tailings were studied.

2. Materials and Methods

2.1. Materials

In this study, the materials used include molybdenum tailing powder, $Ca(OH)_2$, natural gypsum, tap water, and a polycarboxylate-type superplasticizer. $Ca(OH)_2$ was used in its reagent grade, as provided by China Beijing Sinopharm Chemical Reagent Co., Ltd. The molybdenum tailings were provided by a molybdenum mine enterprise in China. In order to understand the content of the main substances contained in the test raw materials, the chemical component analysis mainly used the EDTA dissolution method and a 721 spectrophotometer for determinations. The chemical compositions of the molybdenum tailings and natural gypsum are presented in Tables 1 and 2, respectively.

Table 1. Chemical composition of molybdenum tailings (wt%).

Composition	SiO$_2$	Al$_2$O$_3$	Fe	K$_2$O	MgO	CaO	Na$_2$O	TiO$_2$	P$_2$O$_5$	MnO	Loss	S
Molybdenum tailings	69.24	10.07	3.86	4.89	0.89	2.14	1.99	0.68	0.20	0.17	1.45	0.38

Table 2. Chemical composition of natural gypsum (wt%).

Composition	SiO$_2$	Al$_2$O$_3$	Fe	K$_2$O	MgO	CaO	SO$_3$	K$_2$O	TiO$_2$	P$_2$O$_5$	MnO	Loss
Natural gypsum	1.07	0.29	0.855	0.04	1.43	48.76	43.21	0.04	0.02	0.02	0.009	1.45

2.2. Characteristics of Molybdenum Tailings

The XRD measurements of the molybdenum tailing powder were taken using a Japan Tokyo Rigaku D/MAX-RC12KW diffractometer using Cu Kα radiation at 40 kV and 150 mA, with 2θ = 5°–90°. As shown in Table 1, molybdenum tailing powder consists of SiO$_2$, Al$_2$O$_3$, K$_2$O, Fe, CaO, Na$_2$O, and TiO$_2$. According to the XRD analysis, the molybdenum tailing powder was comprised of quartz, feldspar, magnetite, chlorite, mica, and pyroxene, as shown in Figure 1. Based on the chemical composition analysis results in Table 1, the content of SiO$_2$ in the molybdenum tailings was 69.24%, the content of Al$_2$O$_3$ was 10.07%, and the total amount of K$_2$O + Na$_2$O was 6.88%. It can be preliminarily inferred that the mineral composition of the molybdenum tailings was mainly quartz and feldspar, and the 3.86% Fe in the molybdenum tailings may mainly came from magnetite and pyroxene.

The particle size distribution of the molybdenum tailing powder prepared by grinding the original molybdenum tailings with a laboratory ball mill was determined using a surface area analyzer. The powder had a Blaine fineness of 934.2 m^2/kg.

To ensure that the molybdenum tailings were nonhazardous, the extraction toxicity of the molybdenum tailings was examined in accordance with the Chinese standard GB/T

5085.3-2007: "Identification standards for hazardous wastes-identification for extraction toxicity." The concentration of contaminants, including Cu, Pb, Zn, Ni, Cd, Cr, As, and Hg, in the leachate of the molybdenum tailings was analyzed through inductively coupled plasma atomic emission spectroscopy. The measurement results and regulatory limits specified by GB/T 5085.3-2007 are presented in Table 3. All the contaminants exhibited concentrations well below the regulatory limits, as shown in Table 3. Therefore, the molybdenum tailings used in this study can be considered nonhazardous industrial waste in terms of the extraction toxicity and can be used in cementitious materials.
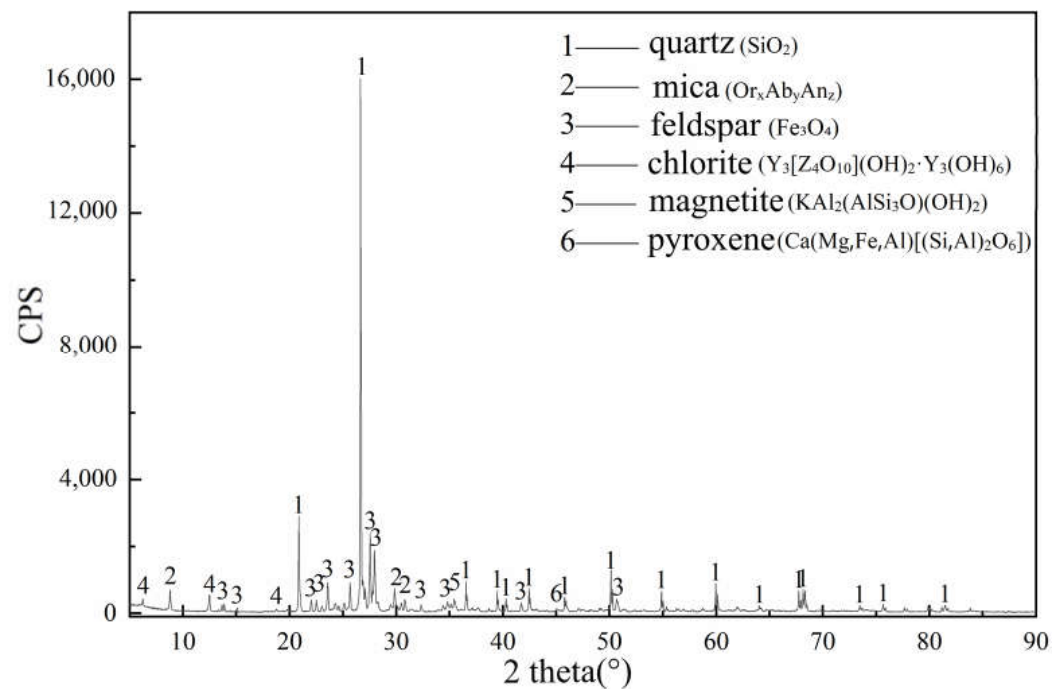

Figure 1. XRD spectrum of molybdenum tailings.

Table 3. Contaminant concerns of molybdenum tailings.

Contaminant	Cu	Pb	Zn	Ni	Cd	Cr	As	Hg
Regulatory level (mg/L)	100	5	100	5	1	5	5	0.1
Leachable concentration of contaminants in molybdenum tailing powder (mg/L)	<0.01	<0.05	<0.006	<0.01	0.004	<0.01	<0.01	<0.001

It should be noted here that molybdenum tailings may be highly radioactive, which may limit their applications. In this study, the radioactivity of the used molybdenum tailings was measured in accordance with GB6566, and the result is presented in Table 4. The results showed that the radioactivity of the molybdenum tailing powder was below the regulatory limitations.

Table 4. Radionuclides detected in the molybdenum tailings (Bq/kg).

Index	^{40}K	^{226}Ra	^{232}Th	IRa	Ir
Radionuclide of molybdenum tailing powder	1249.94	32.29	42.29	0.2	0.6
Limitation of GB6566				≤ 1.0	Ir ≤ 1.0

The IRa (internal exposure index) and Ir (external exposure index) should be less than 1.0, in accordance with GB6566, and are calculated as follows: IRa = $C_{Ra}/370 + C_{Th}/260 + C_{K}/4200$, Ir = $C_{Ra}/200$, 1σ (uncertainty of measurement) $\leq$ 20%.

2.3. Specimen Preparation and Testing

The dried molybdenum tailings were mechanically milled in an SMΦ500 × 500 ball mill. The amount of molybdenum tailings added each time was 5 kg. Samples were taken every 15 min to test their specific surface area and particle size distribution. Field emission SEM was used to conduct microscopic analysis and detection of molybdenum tailing powder for grinding times of 15, 30, 45, 60, 75, and 90 min.

The paste mixture was designed with the following composition: 91 wt% ground molybdenum tailings (with a specific surface area of 934.2 m^2/kg), 6 wt% $Ca(OH)_2$, and 3 wt% natural gypsum. A superplasticizer with a mass ratio of 0.3% was added to the mixture. Water was also added to the mixture in a water/solid ratio of 0.2. After sufficient mixing, nine specimens measuring 30 × 30 × 50 mm^3 were cast for compression tests. All specimens were demolded at the curing age of 24 h in a standard curing chamber at a temperature of 20 °C ± 2 °C and relative humidity of 95% ± 2% until the predesigned age of testing.

The compressive strengths of the hardened paste specimens were measured at the ages of 3, 7, and 28 days. Three specimens were tested at each age. The hydration products of the paste specimens at the ages of 3, 7, and 28 days were evaluated via XRD, Fourier transformed infrared (FTIR) spectroscopy, and SEM.

The XRD measurements of the pastes were taken using a Rigaku D/MAX-RC12KW diffractometer, using Cu Kα radiation at 40 kV and 150 mA, with 2θ = 5°–90°. The FTIR measurements were taken with a Nicolet Nexus 670 spectrometer, and the spectrum scope was set to a range of 4000–400 cm^{-1} with a resolution factor of 0.01 cm^{-1}. The morphology and microstructure of the pastes were observed using a SUPPATM55 SEM.

3. Results

3.1. Specific Surface Area, Characteristic Particle Size, and Morphological Change of Molybdenum Tailings at Different Grinding Times

Table 5 shows the specific surface area test results of the molybdenum tailings with different grinding times. Table 6 shows the characteristic particle size of the molybdenum tailings with different grinding times.

Table 5. Specific surface area of molybdenum tailings with different grinding times.

Grinding Time (min)	0	15	30	45	60	75	90
Specific surface area (m^2/kg)	67.2	367.0	552.7	730.6	934.2	775.1	633.9

Table 6. Characteristic particle size of molybdenum tailings with different grinding times.

Grinding Time (min)	Characteristic Particle Size (μm)		
	D10	D50	D90
0	11.726	141.911	371.131
15	1.648	12.485	48.701
30	1.375	9.846	44.399
45	1.195	7.648	33.448
60	1.041	6.275	29.900
75	0.963	5.434	25.246
90	1.308	10.573	64.568

It can be seen from Table 5 that the particle size of the molybdenum tailings decreases continuously during the grinding process between 15 and 60 min. When the grinding process reaches 60 min, the specific surface area reaches 934.2 m^2/kg; however, after 60 min, the specific surface area decreases, which may be caused by agglomeration between particles during the grinding process.

It can be observed from Tables 5 and 6 that during the grinding process, the molybdenum tailings are micronized due to external grinding action, whereas the fine particles

will agglomerate with each other due to surface adsorption. At the initial stage of grinding, due to the large particles and the small surface energy of the powder, the particles do not agglomerate through mutual attraction. With the prolongation of the grinding time, the particles are continuously refined, and the surface free energy of the particles increases. When grinding exceeds a certain duration, and due to the increase in the surface energy of the powder, the fine particles agglomerate due to surface adsorption [8]. Determining whether the agglomeration phenomenon will affect the continuous increase of the specific surface area can be accomplished by measuring the particle size distribution of the sample using a laser particle size analyzer. If the individual particles of the sample are clustered at the nanometer level, they will not be dispersed by ultrasound and ethanol, and a contradiction phenomenon will occur, which is that the fineness of the sample will continue to increase. However, the particle size distribution test showed that the sample particles became larger instead.

The composition of tailings is complex, the hardness and wear resistance of the various mineral components are different, and the material after grinding does not show a normal distribution. During the initial stage of grinding, the particle size of the minerals was reduced. As grinding continued, the submicron particles of the molybdenum tailings increased significantly. As the particle size decreased, the corresponding specific surface area increased, which is consistent with the test results shown in Table 5. Because this study uses molybdenum tailings to prepare a tailing cementitious material, the national standard requires that the specific surface area of 42.5 ordinary Portland cement should not be less than 300 m^2/kg, and the activity of the molybdenum tailings should be low. When replacing cement with concrete cementitious material, the specific surface area of the molybdenum tailings must be greater than that of ordinary Portland cement. When the grinding time is too long, the grinding cost will increase.

In general, when molybdenum tailings are not milled, the reaction under normal temperature and pressure without a catalyst is slow or difficult. However, after mechanical grinding, the ability of molybdenum tailings to participate in the reaction can be enhanced, and the mechanical properties of the products are improved.

With the reduction of the particle size of the ground molybdenum tailing powder, its specific surface area and surface atom number increase sharply. Additionally, the surface atom coordination is insufficient, resulting in a large number of suspended and unsaturated bonds, which creates a thermodynamically unstable state, i.e., these surfaces have high activity and easily combine with other atoms.

Figure 2 shows the FESEM photos of molybdenum tailings after various grinding durations at 5K× magnification. After grinding for 15 min, most molybdenum tailing particles are long strips and irregular polygonal blocks, with sharp edges and corners. As the grinding duration increases, the size of the tailing particles continues to decrease, and the edges and corners become smooth. At less than 1 μm, the number of ultrafine particles increases. When the grinding time is 60 min, the elongated particles with edges and corners disappear, and many round particles appear. When the grinding time is more than 75 min, the tailing particles exhibit obvious agglomeration.

Based on the above experimental results, the grinding time of molybdenum tailings in the follow-up test was set at 60 min.

3.2. Compressive Strength of Paste Mixtures

The average compressive test results of the hardened paste mixtures at the ages of 3, 7, and 28 days are presented in Table 7. The compressive strength of the hardened paste mixture increased with the curing ages. This finding suggests that the molybdenum tailing powder had certain pozzolanic reactivity.
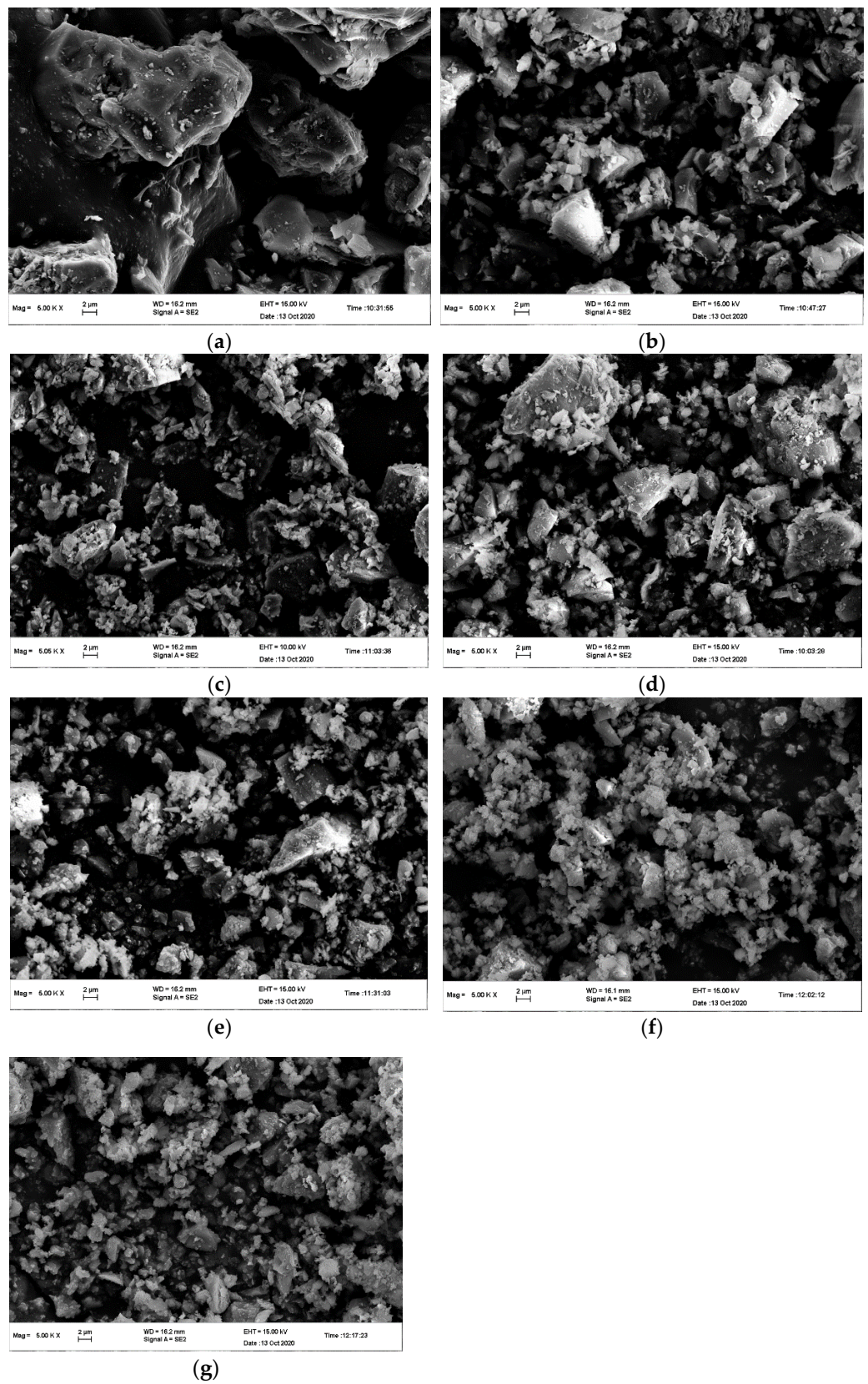
Figure 2. FESEM 5K magnification photos of molybdenum tailings at different grinding times. (**a**) 0 min, (**b**) 15 min, (**c**) 30 min, (**d**) 45 min, (**e**) 60 min, (**f**) 75 min, and (**g**) 90 min.

Table 7. Compressive strength of the hardened paste specimens at various curing ages.

Curing age (days)	3	7	28
Compressive strength (MPa)	1.67	3.17	3.83

3.3. XRD Analyses of Paste Mixtures

The XRD patterns of the original molybdenum tailing powder (DGJJ) and the hardened paste specimens aged for 3, 7, and 28 days are shown in Figure 3. The distinctive peaks ($2\theta = 18.04°$ and $34.04°$) of portlandite became weaker with increasing curing age and disappeared at a curing age of 28 days. The characteristic peak of gypsum ($2\theta = 11.63°$) basically disappeared at the curing age of 3 days, indicating that the gypsum was basically completely consumed at a curing age of 3 days. In addition, the distinctive peaks ($2\theta = 9.16°$ and $15.68°$) of ettringite (AFt) appear at the curing age of 3 days and intensify at the curing age of 28 days. This observation indicates that the amount of ettringite increased with the curing age. The XRD pattern of a typical C-S-H gel tends to form a hump at diffraction angles (2θ) between $26°$ and $34°$ [9]. As shown in Figure 3, a higher background value can be observed in the pattern for the diffraction angles between $26°$ and $34°$ increasing curing age. This observation indicates the formation of more C-S-H gel as the curing process progressed. The formation of ettringite and C-S-H gel explain the strength enhancement (Table 7) of the hardened paste mixture. Table 8 lists the changes in the XRD patterns of typical components at different curing ages in the molybdenum tailing powder and the paste mixtures.
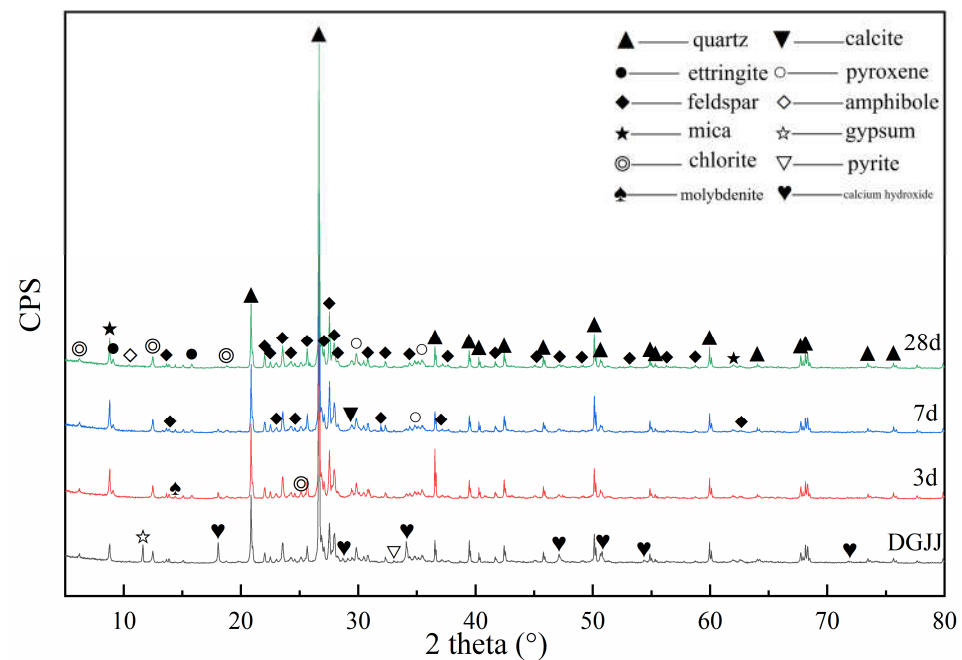
Figure 3. XRD patterns of the molybdenum tailing powder and the paste mixtures at different curing ages.

Table 8. Changes in XRD patterns of typical components at different curing ages.

Mineral Composition	2θ	Original Powder	3 Days	7 Days	28 Days
Portlandite	18.04°; 34.04°	exist	weaken	weaken	disappear
Gypsum	11.63°	exist	disappear	non-existent	non-existent
Ettringite (AFt)	9.16°, 15.68°	non-existent	appear	intensify	intensify
C-S-H gel	Between 26° and 34°	non-existent	appear	intensify	intensify

3.4. SEM Analyses of the Paste Mixtures

SEM was employed to characterize the morphology of the hydration products and the microstructure of the hardened specimens at different ages. The surface microstructures of the fractured surface and inner pores of the paste specimens aged for 3, 7, and 28 days are presented in Figure 4. As shown in this figure, the amount of needle-like phases on the surface of the pores in the paste specimens increased with the increase in the curing age. Further magnification of Figure 4(b1) is given in Figure 4(b2), where the needle-like phase corresponds to AFt crystals. Figure 4(a1,a2) display the presence of several unhydrated molybdenum tailing particles on the broken surface of the paste specimens at the curing age of three days. The comparison of Figure 4(b1) with Figure 4(c1) revealed the formation of more needle-like AFt with the increase in curing age. As shown in Figure 4(c2), the molybdenum tailing particles were coated well with the amorphous C-S-H gel at the curing age of 28 days, resulting in a denser microstructure. Therefore, the amount of AFt and C-S-H gel in the paste specimens increased with the increase in the curing age, resulting in a denser microstructure that contributes to strength enhancement.
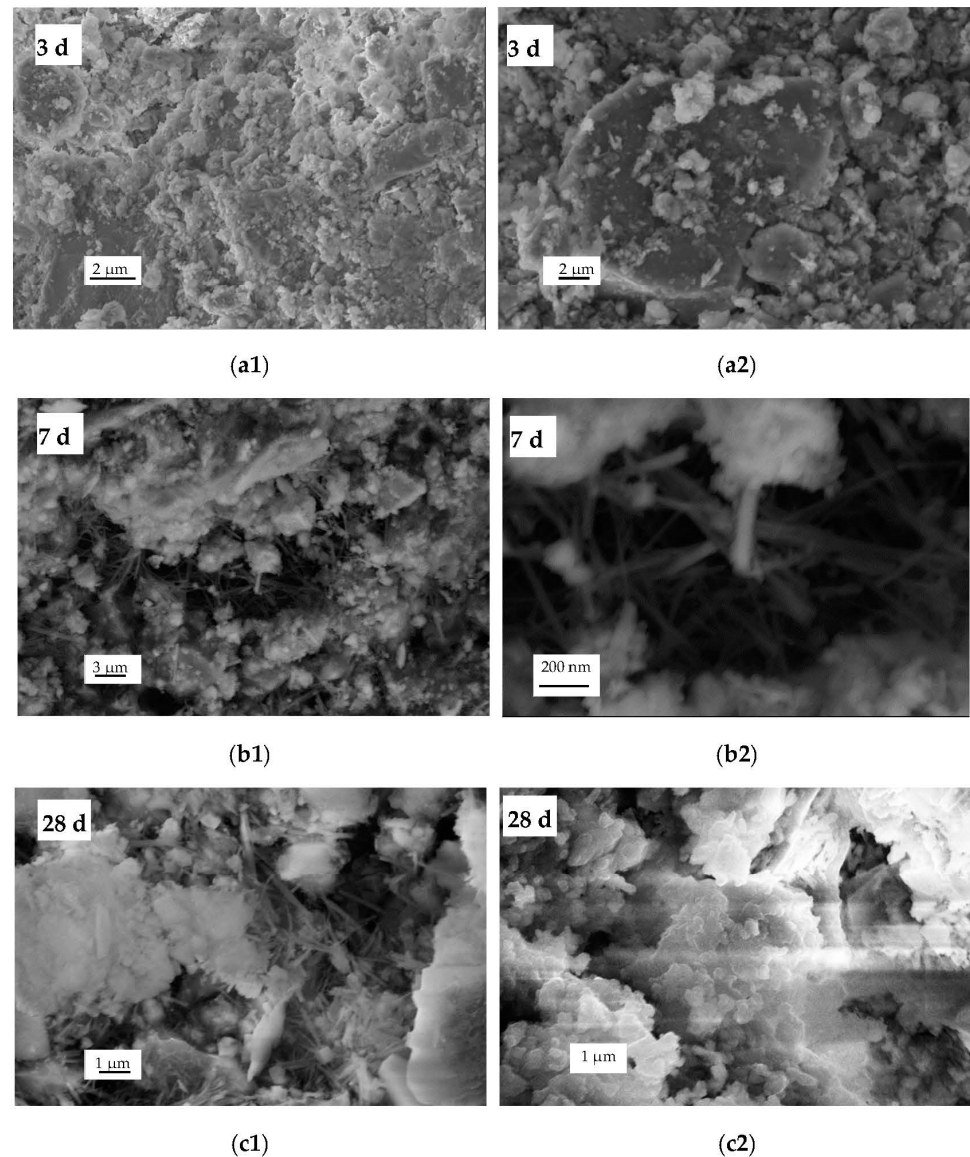

Figure 4. SEM images and EDS spectrum of hydration products at different ages. (**a1,a2**) 3 days, (**b1,b2**) 7 days, (**c1,c2**) 28 days.

3.5. FTIR

Figure 5 shows the FTIR spectra of the hydrated neat cementitious material specimens mixed with ground molybdenum tailings, gypsum, and Ca(OH)$_2$ when cured for 3, 7, and 28 days. The IR spectrum of the dry mixture is also shown as a comparison. As shown in Figure 5, the absorption band between 3800 and 3000 cm^{-1} indicates the stretching vibration of O-H bonds in the different phases of the system. The prominent absorption bands of ~3640 cm^{-1} indicate that the O-H bonds in Ca(OH)$_2$ became weaker and nearly disappeared at the curing age of 28 days [10–13]. This suggests that the hydration reaction consumed most of the Ca(OH)$_2$ when the curing age was prolonged to 28 days.
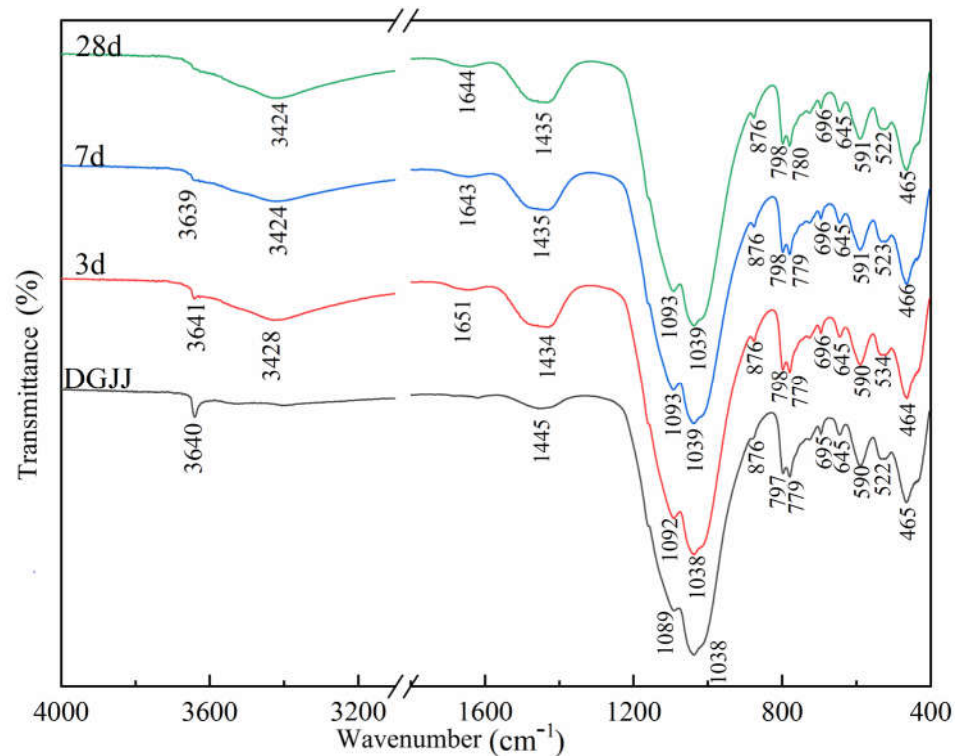

Figure 5. FTIR spectra of the hardened paste specimens at different curing ages.

Similar absorption peaks were also observed at 3428, 3424, and 3424 cm^{-1} in the IR spectra of the specimens cured for 3, 7, and 28 days, respectively. These peaks are the overlaps of the O-H bonds attached to silica and the O-H bonds in ettringite. Interestingly, the wave numbers of the peaks increased from the dry mixture specimen to the specimens cured for three days. This increase indicates that the average bonding energy of the O-H bonds increased continuously from the dry mixture specimen to the specimens cured for three days. It also suggests that the average abstraction forces between the cations in the system and the O-H bonds became increasingly weaker. The combined water in the newly formed ettringite and C-S-H gels was generally less strongly bound to the cations than in well-crystallized silicate minerals. This property resulted in a higher bonding energy of the O-H bonds in the newly formed ettringite and C-S-H gels. Conversely, the increasingly prominent absorption bands between 3800 and 3000 cm^{-1} indicate the occurrence of a hydrating reaction that progressed with the increase in the curing age. This deduction coincides well with the results obtained from the XRD and SEM analyses.

An absorption band of ~1651 cm^{-1}, which is a characteristic of the bending vibration of the O-H bonds of structural or crystallized water, occurred in the spectra of the specimens cured for three days. This peak was mainly due to the newly formed ettringite. Similar absorption peaks also occurred at 1643 and 1644 cm^{-1} in the IR spectra of specimens cured for 7 and 28 days, respectively. The absorption peak appeared in the 3-, 7-, and 28-day

specimens, but not in the dry mixture specimen. This finding indicates that ettringite was generated during the hydration reaction.

Another prominent absorption peak occurred at 1445 cm^{-1} [10,14] due to the original calcite mineral in the molybdenum tailings. This peak is a characteristic of the stretching vibration of CO_3^{2-} in the IR spectrum of the dry mixture. Similar absorption peaks also occurred at 1434, 1435, and 1435 cm^{-1} in the IR spectra of the specimens cured for 3, 7, and 28 days, respectively. Thus, the peaks became slightly more prominent with the increasing curing age; however, the wavenumbers did not change significantly. This observation suggests that new calcite minerals were formed during the curing process by combining with the carbon dioxide in the atmosphere.

The absorption band of ~1089 cm^{-1} is a characteristic of the asymmetric stretching vibration of the S-O bands in the IR spectrum of the dry mixture [15] and is typically due to the original gypsum mineral. The moderately wide range and lack of sharpness of this peak reflect the lower crystalline or multiphase character of gypsum. Similar absorption peaks also occurred at 1092, 1093, and 1093 cm^{-1} in the IR spectra of the specimens cured for 3, 7, and 28 days, respectively. This finding suggests that the peaks became more prominent and their sharpness increased with the increasing curing age; however, the wavenumbers did not change significantly. These changes indicate that the SO_4^{2-} ions were transformed from the gypsum minerals to the ettringite minerals, which are normally well crystallized.

The absorption band at ~876 cm^{-1} characterizes the asymmetric stretching vibration of the Al-O bands in various minerals [16]. This absorption band became increasingly sharper from the dry mixture to the specimens cured for 3 to 7 to 28 days. This observation indicates that the Al-O bands increased continuously in one well-crystallized mineral, while the Al-O bands in the other minerals disappeared. The above XRD and SEM analyses suggest that the concentration of Al-O bands was mainly caused by the crystallization of ettringite.

The last noticeable absorption band is located at ~464 cm^{-1} and characterizes the asymmetric bending vibration of Si-O-Si bands in various complicated silicate minerals and typically in C-S-H gels [17,18]. This absorption band became increasingly sharper from the dry mixture to the specimens cured for 3 to 7 to 28 days. This finding suggests that the total amount of C-S-H gel increased continuously, while other silicate minerals were being consumed.

4. Discussion

The gelling system comprises numerous ultrafine molybdenum tailing particles. Tailings are aluminosilicate systems connected by several silica and alumina tetrahedrons. Cations, such as Ca^{2+} and Mg^{2+}, are distributed around the silica and alumina tetrahedrons to balance charges. Under the action of an alkaline solution of slurry containing calcium hydroxide, the cations on the surface of the tailing particles are first dissolved into the solution. This intensifies the charge imbalance between the remaining silicon-oxide and aluminum-oxide tetrahedrons, resulting in the breakage of the aluminum-oxide bond of the aluminum-oxide tetrahedron. This aluminum-oxide tetrahedron is dissolved from the surface of tailing particles in the form of meta-aluminate and tends to form a solution balance between the surface of tailing particles and the solution.

$$AlO_2^- + 2OH^- + 2H_2O = [Al(OH)_6]^{3-} \tag{1}$$

Gypsum rapidly dissolves Ca^{2+} and SO_4^{2-} when it meets water. $[Al(OH)_6]^{3-}$ formed in Equation (1) combines with Ca^{2+} and SO_4^{2-} in the solution to form ettringite. The reaction equation is as follows:

$$2[Al(OH)_6]^{3-} + 6Ca^{2+} + 3SO_4^{2-} + 26H_2O = Ca_6Al_2(SO_4)_3(OH)12 \cdot 26H_2O \tag{2}$$
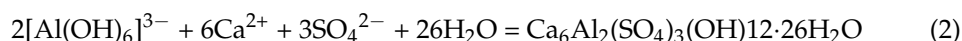
With the continuous formation of ettringite, the dissolution balance of meta-aluminate between the surface and solution of tailing particles is constantly broken, promoting the continuous migration of aluminum-oxide tetrahedra from the surface of tailing particles.

The migration of aluminum-oxide tetrahedra from the surface of tailing particles destroys the connection between the silicon-oxide tetrahedron and the aluminum-oxide tetrahedron. This causes the polymerization degrees of silicon-oxide and aluminum-oxide tetrahedra on the surface of tailing particles to drop rapidly, which results in the significantly increased activity of residual silicon-oxide and aluminum-oxide tetrahedra. In addition, the C-S-H gel is constantly formed in the slurry solution rich in Ca^{2+}. Therefore, there may be a synergistic process of ettringite and C-S-H gel in the cementitious system containing several ultrafine molybdenum tailings, $Ca(OH)_2$, and gypsum.

5. Conclusions

This study on the mechanical activation of molybdenum tailings shows that the particle size of molybdenum tailings decreases continuously during the grinding process between 15 and 60 min, and the specific surface area increases from 367 to 932.4 m^2/kg. With the extension of grinding time, the mineral particles are gradually decreased in size and smoothed from larger angular particles. After the grinding time exceeds 75 min, obvious agglomeration occurs between the particles, and the specific surface area decreases to 633.9 m^2/kg at 90 min. This study demonstrates the pozzolanic reactivity of molybdenum tailing powder at a temperature of 20 °C ± 2 °C. The paste specimens containing 91 wt% molybdenum tailing powder, 3 wt% natural gypsum, and 6 wt% $Ca(OH)_2$ exhibit compressive strengths of 1.67, 3.17, and 3.83 MPa, respectively, at the curing ages of 3, 7, and 28 days, respectively. The AFt and C-S-H gel are formed in the molybdenum tailing powder–gypsum–$Ca(OH)_2$ paste, and the amount of AFt and C-S-H gel in the paste specimens increases with increasing curing ages. This explains the strength enhancement of the paste. Thus, the findings of this study suggest the synergistic process of ettringite and C-S-H gel in the cementitious system containing several ultrafine molybdenum tailings, $Ca(OH)_2$, and gypsum.

Based on the previous research results on the pozzolanic activity and hydration products of other high-silicon-type tailings and single minerals [19–21], it can be preliminarily judged that molybdenum tailings with high silicon content similar to this study can produce pozzolanic activity after a certain degree of grinding treatment, and its main hydration products will also be mainly ettringite and CSH gel.

Author Contributions: Conceptualization, B.G., Z.W. (Zongwen Wang), and S.S.; methodology, B.G. and S.S.; software, K.W. and J.F.; validation, B.G., Z.W. (Zhenjiang Wen), and X.G.; formal analysis, B.G. and K.W.; investigation, B.G.; resources, Z.W. (Zongwen Wang) and S.S.; data curation, B.G.; writing—original draft preparation, B.G.; writing—review and editing, B.G.; visualization, B.G.; supervision, S.S.; project administration, Z.W. (Zongwen Wang) and S.S.; funding acquisition, Z.W. (Zongwen Wang) and S.S. All authors have read and agreed to the published version of the manuscript.

Data Availability Statement: The data presented in this study are available from the corresponding author upon request.

Conflicts of Interest: The authors declare no conflict of interest. The funders had no role in the design of the study; in the collection, analyses, or interpretation of data; in the writing of the manuscript; or in the decision to publish the results.

References

1. Zhang, W. Progress of research on dressing technology of molybdenum ores. *China Molybdeunm Ind.* **2009**, *33*, 1–6.
2. Di, Y.; Cui, X.; Pang, H. Preparation of a new type of lightweight building thermal insulation material mixed with tailings. *Concr. Cem. Prod.* **2016**, 66–69.
3. Di, Y.; Cui, X.; Li, C. Preparation of foamed cement thermal insulation material mixed with molybdenum tailings. *New Build. Mater.* **2016**, 10–13.
4. Di, Y.; Cui, X. Preparation of high-performance concrete mixed with tailings. *J. Shangluo Univ.* **2015**, 32–36.
5. Guo, X.; Yang, Y.; Lin, H. Study on the preparation of road cement clinker using molybdenum slag. *New Build. Mater.* **2011**, 21–34.
6. Cui, X.; Di, Y.; Nan, N. Experimental Study on Molybdenum Tailings Aggregate Concrete. *Concr. Cem. Prod.* **2016**, 84–87.
7. Cui, X.; Di, Y.; Nan, N. Preparation of high-performance concrete mixed with molybdenum tailings. *Met. Mines* **2017**, 192–196.
8. Yang, N. Mechanochemical processes and effects (I)—Mechanochemical effects. *J. Build. Mater.* **2000**, *3*, 19–26.
9. Bensted, J.; Barnes, P. *Structure and Performance of Cements*, 2nd ed.; Spon Press: New York, NY, USA, 2002.
10. Ylmén, R.; Jäglid, U.; Steenari, B.M.; Panas, I. Early hydration and setting of Portland cement monitored by IR, SEM and Vicat techniques. *Cem. Concr. Res.* **2009**, *39*, 433–439. [CrossRef]
11. Silva, D.A.; Roman, H.R.; Gleize, P.J.P. Evidences of chemical interaction between EVA and hydrating Portland cement. *Cem. Concr. Res.* **2002**, *32*, 1383–1390. [CrossRef]
12. Lee, T.C.; Wang, W.J.; Shih, P.Y.; Lin, K.L. Enhancement in early strengths of slag-cement mortars by adjusting basicity of the slag prepared from fly-ash of MSWI. *Cem. Concr. Res.* **2009**, *39*, 651–658. [CrossRef]
13. Mollah, M.Y.A.; Yu, W.; Schennach, R.; Cocke, D.L. A Fourier transform infrared spectroscopic investigation of the early hydration of Portland cement and the influence of sodium lignosulfonate. *Cem. Concr. Res.* **2000**, *30*, 267–273. [CrossRef]
14. Trezza, M.A.; Lavat, A.E. Analysis of the system $3CaO \cdot Al_2O_3 - CaSO_4 \cdot 2H_2O - CaCO_3 - H_2O$ by FT-IR spectroscopy. *Cem. Concr. Res.* **2001**, *31*, 869–872. [CrossRef]
15. Carmona-Quiroga, P.M.; Blanco-Varela, M.T. Ettringite decomposition in the presence of barium carbonate. *Cem. Concr. Res.* **2013**, *52*, 140–148. [CrossRef]
16. Hughes, T.L.; Methven, C.M.; Jones, T.G.; Pelham, S.E.; Fletcher, P.; Hall, C. Determining cement composition by Fourier transform infrared spectroscopy. *Adv. Cem. Based Mater.* **1995**, *2*, 91–104. [CrossRef]
17. Yu, P.; Kirkpatrick, R.J.; Poe, B.; McMillan, P.F.; Cong, X. Structure of calcium silicate hydrate (C-S-H): Near-, mid-, and far-infrared spectroscopy. *J. Am. Ceram. Soc.* **1999**, *82*, 742–748. [CrossRef]
18. Lodeiro, I.G.; Macphee, D.E.; Palomo, A.; Fernández-Jiménez, A. Effect of alkalis on fresh C-S-H gels. FTIR analysis. *Cem. Concr. Res.* **2009**, *39*, 147–153. [CrossRef]
19. Geng, B.Y.; Ni, W.; Wang, J.J.; Qiu, X.J.; Huang, X.Y. An Initiative Investigation of the Pozzolanic Reaction of Ground Lead-Zinc Ore Tailings. *Int. J. Earth Sci. Eng.* **2015**, *8*, 1271–1278.
20. Geng, B.Y.; Ni, W.; Wang, J.J.; Qiu, X.J.; Cui, X.; Ren, C.; Xing, Y. Pozzolanic Reactivity and Hydration Products of Hedenbergite. *Chem. Eng. Trans.* **2017**, *62*, 943–948.
21. Geng, B.Y.; Ni, W.; Wang, J.J.; Qiu, X.J.; Cui, X.; Ren, C.; Xing, Y. Pozzolanic reactivity and hydration products of Quartz. *J. Mines Met. Fuels* **2017**, *65*, 641–647.